ELSEVIER

journal homepage: www.intl.elsevierhealth.com/journals/cmpb

Enhancement of lung sounds based on empirical mode decomposition and Fourier transform algorithm

Ashok Mondal *, *Poulami Banerjee*, *Ajay Somkuwar*

Department of Electronics and Communication Engineering, National Institute of Technology, Bhopal, India

ARTICLE INFO

Article history:
Received 28 May 2016
Received in revised form
13 September 2016
Accepted 24 October 2016

Keywords:
Empirical mode decomposition
Fast Fourier transform
Heart sound
Lung sound
Power spectral density
Spectrogram

ABSTRACT

Background and objective: There is always heart sound (HS) signal interfering during the recording of lung sound (LS) signals. This obscures the features of LS signals and creates confusion on pathological states, if any, of the lungs. In this work, a new method is proposed for reduction of heart sound interference which is based on empirical mode decomposition (EMD) technique and prediction algorithm.

Method: In this approach, first the mixed signal is split into several components in terms of intrinsic mode functions (IMFs). Thereafter, HS-included segments are localized and removed from them. The missing values of the gap thus produced, is predicted by a new Fast Fourier Transform (FFT) based prediction algorithm and the time domain LS signal is reconstructed by taking an inverse FFT of the estimated missing values.

Results: The experiments have been conducted on simulated and recorded HS corrupted LS signals at three different flow rates and various SNR levels. The performance of the proposed method is evaluated by qualitative and quantitative analysis of the results.

Conclusions: It is found that the proposed method is superior to the baseline method in terms of quantitative and qualitative measurement. The developed method gives better results compared to baseline method for different SNR levels. Our method gives cross correlation index (CCI) of 0.9488, signal to deviation ratio (SDR) of 9.8262, and normalized maximum amplitude error (NMAE) of 26.94 for 0 dB SNR value.

1. Introduction

Lung sounds are produced by vortical and disruptive flow of air [1] [2] within lung airways during inspiration and expiration process [3]. Heart sounds are created by the flow of blood into and out of the heart and by the movement of structures involved in the control of this flow [4] [5], [6]. The maximum information of HS signal lies in the frequency range of 20–150 Hz [7] [8], [9]. However, the frequency range of HS signal including murmur sound extending from 20 Hz to 500 Hz or higher due to its impulsive nature. Heart sounds are clearly audible in lung sounds recorded on the anterior chest and may be heard to a lesser extent in lung sounds recorded over posterior lung lobes. After the invention of stethoscope by Laennec [10] in 1816, it is employed as a primary tool to detect lung

* *Corresponding author.* Department of Electronics and Communication Engineering, National Institute of Technology, Bhopal, India.
E-mail address: ashokrpe@gmail.com (A. Mondal).

http://dx.doi.org/10.1016/j.cmpb.2016.10.025
0169-2607/

diseases, but traditional auscultation with a stethoscope constraints a diagnostic test primarily due to the interference of the heart sound with lung sounds. The heart sound signal interference obscures the interpretation of lung sounds and lead to an inaccurate diagnostic result of the lung diseases. It is highly desirable, for accurate assessment of the lung diseases based on lung sound information, to remove the heart sound interference [11–24]. The secondary drawback of the auscultation technique is the limitation of the human auditory system [25]. A less experienced physician may find it more difficult to interpret LS in presence of HS. However, this problem may be solved by the skilled and experienced physician. It is experimentally observed that besides HS signal some unwanted components appear in LS records due to improper placement of stethoscope, and this problem can be avoided by proper placement of stethoscope under the supervision of an expert chest specialist. Apart from this, we have noticed that LS records are affected by environmental noise such as fan noise, babble noise, car noise etc. This problem can be avoided by recording the LS in a quiet environment. The methods used for HS separation from LS signal remained an area of interest among researchers. Methods like adaptive filtering [26–31], wavelet-based filtering [32–36], and short time Fourier transform (STFT) based approach [37] [38], have been tried with some success. Most of the filtering approaches follows a preprocessing step of HS segmentation algorithm [39–44]. The performance of HS detection algorithms depend on the statistical properties of signals and characteristics of basis function employed to decompose them. These conventional filtering approaches use a fixed type of basis function or mother wavelet irrespective of the signal characteristics and require human intervention. In order to improve the performance of the filtering technique, we need an adaptive basis function which is adjustable by only the signal properties. In this paper, we propose a new method based on adaptive EMD technique and FFT based prediction algorithm for separation of HS signal from LS signal. The EMD technique decomposes the signal into a number of different time scales or intrinsic mode functions (IMFs) by exploring the statistical properties of the signal. This allows us to filter signal components individually instead of filtering the original signal. It is found that certain components of the signal highlight the presence of interference or noise in the LS signal more. Thus, it becomes easier to remove them from the signal using the EMD technique. Studies shows that embedded components are more relevant than signal as a whole for denoising the LS signal. In addition, the proposed method has ability to remove efficiently the HS interference from LS signals without any need for a reference signal, unlike the technique introduced by Iyer et al. [26]. The LS signal obtained by conventional filtering approaches contains a significant amount of HS information, and it may lead to misinterpretation of pulmonary dysfunction. In this study, we propose an FFT based prediction algorithm to estimate the missing LS values corresponding to the gaps produced due to removal of HS segments. The HS-included segments are identified by Hilbert Heron algorithm (HHA) [45].

The rest of this paper is organized as follows. A brief description of the empirical mode decomposition (EMD) technique is presented in section II. Section III describes in details the proposed enhancement technique. The experimental database and certain implementation issues are described in section IV. Section V illustrates the experimental results and comparisons with an earlier technique. The conclusion of the chapter is given in section VI.

2. Theoretical background

2.1. *The empirical mode decomposition*

The concept of empirical mode decomposition was developed by N. Huang et al. for analysis of the non-stationary and non-linear data [46]. This algorithm is adaptive in nature and circumvents the disadvantages of conventional techniques such as DFT, STFT, WT, etc. The procedure of computing IMFs from an LS signal $x(n)$ is summarized as follows:

(1) The extreme points of the signal are selected by counting the sign changes over the derivative of $x(n)$. A sample in a signal is a maxima point if its adjacent preceding and succeeding slopes are positive and negative, respectively and it becomes a minima point for vice versa. If we consider a sample value s_i then it will be a maximum valued point for

$$\frac{d(s_i)}{dn} = 0 \,||\, \frac{d(s_{i-1})}{dn} > 0 \,||\, \frac{d(s_{i+1})}{dn} < 0$$

and will be a minimum valued point for

$$\frac{d(s_i)}{dn} = 0 \,||\, \frac{d(s_{i-1})}{dn} < 0 \,||\, \frac{d(s_{i+1})}{dn} > 0$$

(2) Computation of the lower and upper envelopes: The lower and upper envelopes are produced using the local minima and maxima with the help of cubic spline interpolation method, and they are designated as $e_{min}(n)$ and $e_{max}(n)$, respectively.

(3) Calculation of the mean of the lower and the upper envelopes, $m_e(n)$

$$m_e(n) = \frac{e_{max}(n) + e_{min}(n)}{2}.$$

(4) Computation of the deviation of the data $x(n)$ from the average $m_e(n)$ of the envelopes and designate it as $d_1(n)$,

$$d_1(n) = x(n) - m_e(n).$$

(5) $d_1(n)$ is not necessarily an IMF. Sifting process is employed as many times as required to extract an IMF, as shown in step 6.

(6) Substitution of the original signal $x(n)$ by $d_1(n)$ and iteration of the steps 1 to 4 until the stopping criterion is met and it is calculated by limiting the normalized standard deviation, as follows

$$NSD_k = \frac{\sum_{n=0}^{T} |d_{1,k-1}(n) - d_{1,k}(n)|^2}{\sum_{n=0}^{T} [d_{1,k-1}(n)]^2}$$

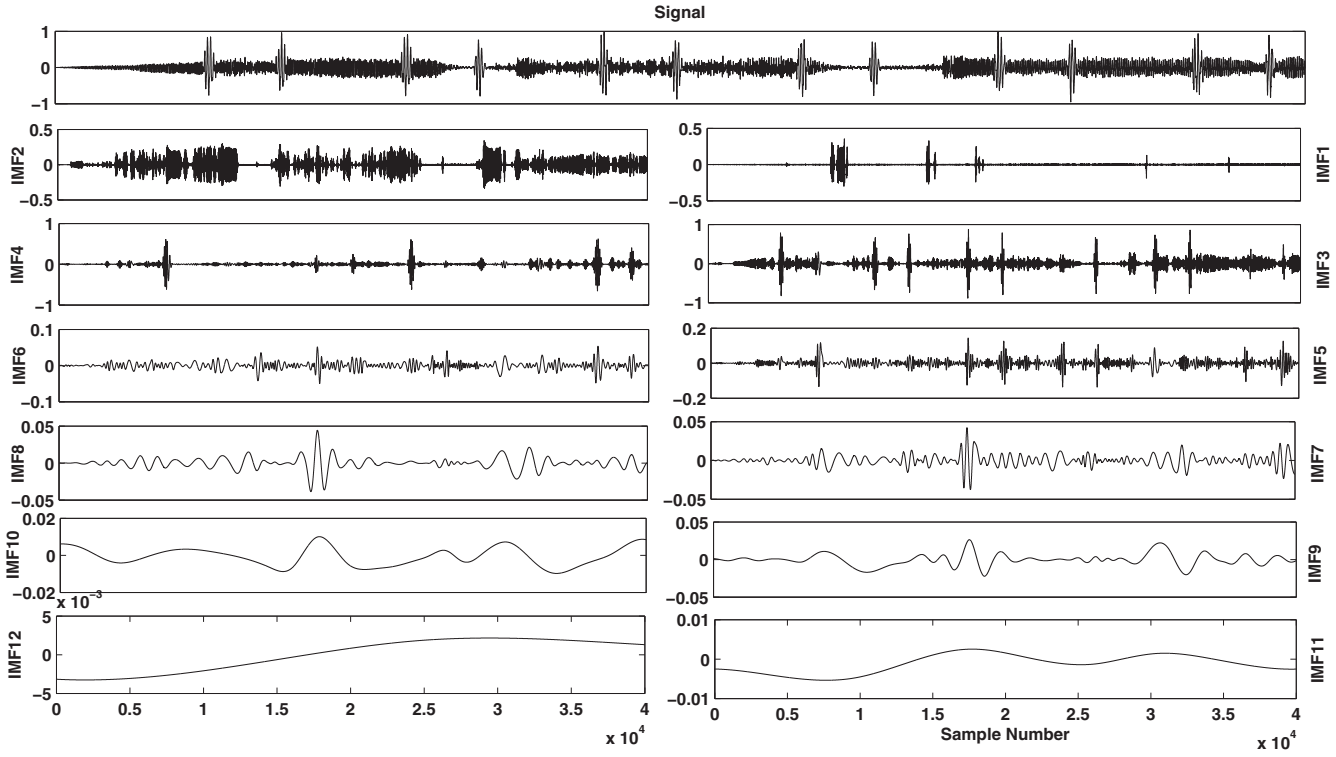

Fig. 1 – Signal $x(n)$ on the top and its eleven IMF components (IMF_1 to IMF_{11}) and the residual (IMF_{12}) on the bottom obtained by EMD method from mixed signal $x(n)$.

where *NSD* is usually set as δ whose value lies in the range of 0.2 to 0.3, and k is the total number of sifts.

(7) Once the k number of sifts results in an IMF, defined as

$$b_1(n) = d_{1k}(n).$$

(8) We obtain the residue $r_1(n)$

$$r_1(n) = x(n) - b_1(n).$$

(9) We consider $r_1(n)$ as a new data set and iterate the steps 1–8 for M times until the residual component $r_M(n)$ converts into a monotonic function.

(10) Finally,

$$x(n) = \sum_{i=0}^{M} b_i(n) + r_M(n)$$

where $b_i(n)$ stands for the i-th *IMF* and $r_M(n)$ represents the final residual component. Empirical mode decomposition technique is an iterative process. In this approach, the locally lowest frequency components are left out from the signal, resulting in decrease of energy in the successive components as shown in Fig. 1.

3. Methodology

The basic principle of the proposed HS interference reduction method presented here is the extraction of HS corrupted segments from the IMFs which are generated from the impure LS signal $x(n)$ with the help of EMD technique. Before removal of HS-included segments, it is necessary to identify their peak locations. The peak positions of HS components within noisy LS signal are detected by a biomedical domain feature based method that was introduced in Ref. [45]. The identified HS peaks are bounded and extracted from every IMF, and the missing LS values corresponding to the created gaps are estimated using an FFT based prediction algorithm. The proposed method comprises of four parts: an IMF generation scheme, a HS localization scheme, a missing value prediction scheme and an LS reconstruction scheme. The whole process is described in Fig. 2 using a block diagram. First, HS peaks in the corrupted LS signal are localized and bounded by employing a suitable HS localization algorithm [45]. After the detection of HS-included segments, these corrupted segments are removed from all IMFs. As a result, the IMFs of the mixed signal contain only LS information along with several gaps which are created due to removal of HS contaminated segments from LS record. The missing samples of IMF component are estimated using a new FFT based prediction algorithm. Finally, the LS signal is reconstructed by summing up all IMFs which are free of HS interference.

3.1. *Generation of intrinsic mode functions*

Instead of the original mixed sound signal, its constituting components are more relevant in reduction of HS interference from LS signal [47] [48], [49]. In this experiment, the components comprising of the noisy LS signal is extracted using an adaptive decomposition technique that is free from human

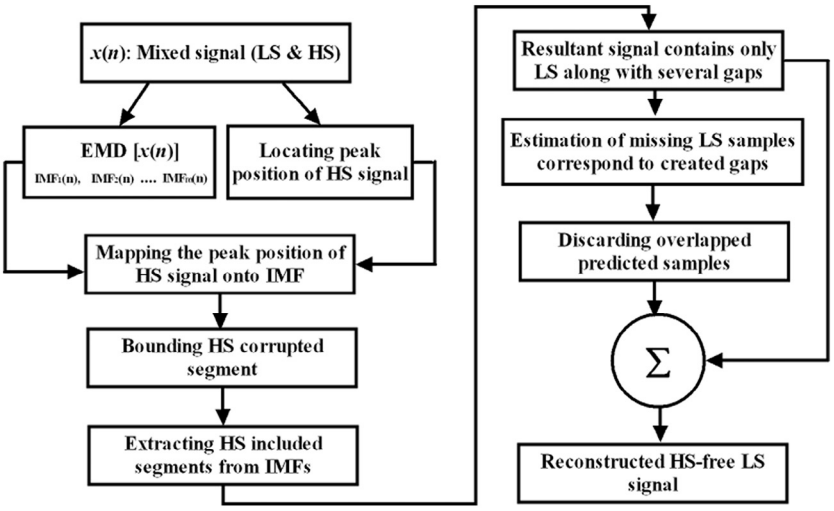

Fig. 2 – Block diagram of the proposed method showing the sequence of steps required for the reconstruction of the pure LS signal.

intervention. The steps involved in generation of IMFs have been discussed in subsection 2.1. The waveforms of one mixed signal of LS and HS and its IMF components are shown in Fig. 1.

3.2. *HS localization in LS*

Heart sound interference is unavoidable in lung sound recordings. The effect of HS interference over LS signal varies with breathing flow rate as shown in Fig. 3. The LS information is obscured to a great extent for low flow in comparison to medium and high flow rates. To reduce the HS interference, HS localization is an important preprocessing step of LS enhancement method. The LS is corrupted by HS for the certain regions instead of the entire signal. In the preprocessing stage, first the HS peaks are identified and then their boundaries are estimated using a HS localization technique [45].

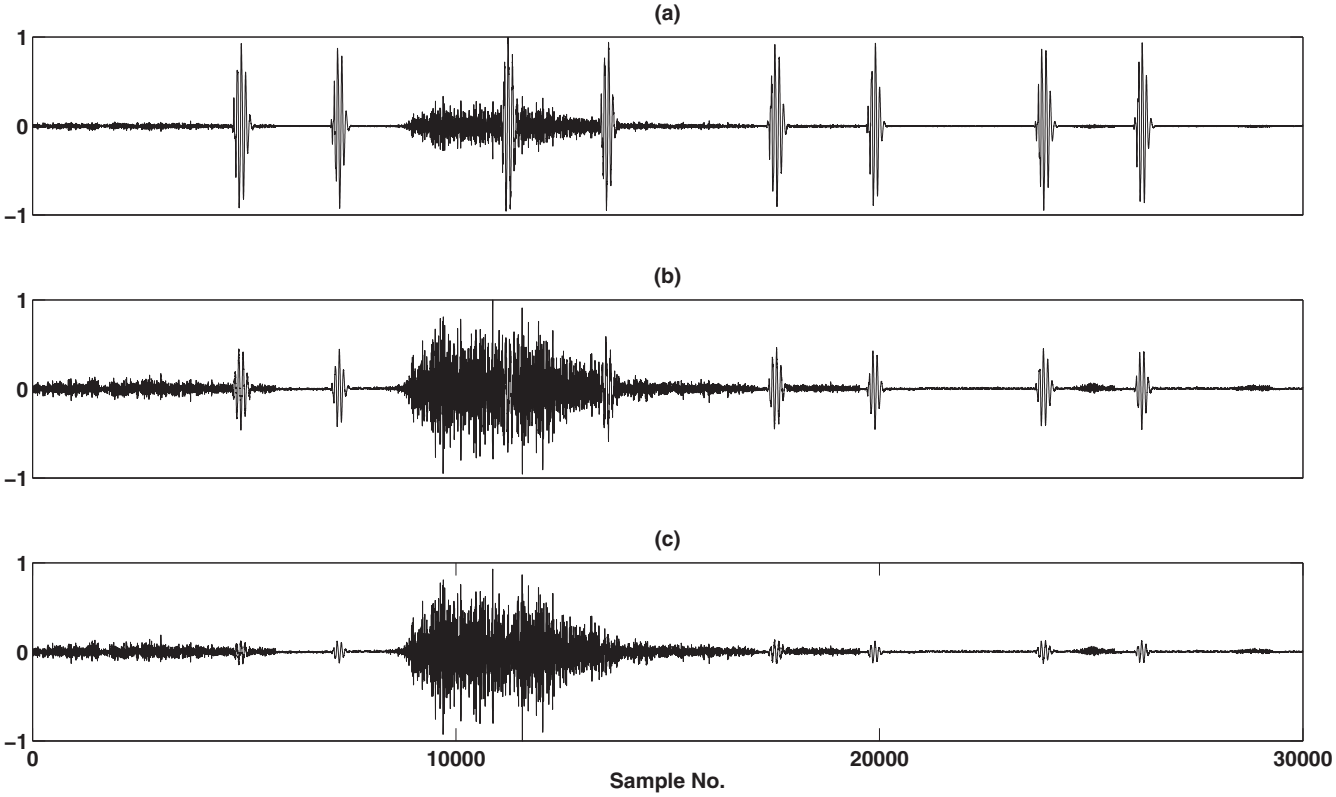

Fig. 3 – Variation of flow rate: normalized waveform of a HS corrupted LS signal at (a) low flow rate, (b) medium flow rate and (c) high flow rate.

3.2.1. *Detection of peak locations of HS signal*

The peak location identification of HS signal is one of the important steps for reduction of HS interference from LS signals. In this context, researchers have developed many algorithms for localization of HS peaks in noisy LS signals [34] [37], [50], [51–54]. In this work, a medical domain feature based method is used for detection of HS peak position within the LS signals. The peak detection algorithm is discussed elaborately in Ref. [45]. The summary of the peak detection algorithm is given next.

3.2.2. *Boundary estimation of HS-included segments*

The next step in HS localization method is estimation of the boundary of the HS corrupted segment. The HS signals are produced due to the circulation of blood through heart. Hence, the HS signal is extended to a certain range in both directions of its peak. Study shows that the HS is extended in forward and backward directions by 100 ms and 50 ms from the peak HS [55], respectively and it is illustrated in Ref. [49]. The HS boundary estimation algorithm is explained in details in Ref. [45]. A summary of this algorithm is given next.

3.3. *Prediction of missing samples*

In this stage, first the detected HS-included segments are removed from the corrupted LS signal. As a result, the resultant signal $sig_{res}(n)$ contains only LS information along with a number of gaps as shown in Fig. 4 (b). The length of these gaps depends on the duration of the HS components. The values of the samples corresponding to these gaps are unknown. In this work, a novel FFT based prediction algorithm has been introduced for prediction of the values of the unknown samples using their neighboring known samples values. The prediction approach comprises of two steps:

Step 1: Calculate the length of the created gap: Each HS corrupted segment has a certain duration. After removal of HS included segments, a number of null valued regions are produced in between the LS segments as shown in Fig. 4 (b). The duration of these intervals can be calculated by using their start and end point locations coordinates. Let us consider the starting and end points location

Algorithm 1: *HS Peak Detection*

Normalize the mixed signal of LS and HS.
Filter the normalized mixed signal using a $10th$ *order Butterworth low pass filter with a cutoff frequency* 150 *Hz.*
Compute the Hilbert envelope of the filtered signal using Hilbert transform.
Detect the peaks in the envelope signal by applying smoothing and differential operations.
Identify the HS peaks using a selection criteria based on Heron's triangular formula.

Algorithm 2: *Boundary Estimation of HS Peak*

Take Hilbert envelope of mixed signal of LS and HS.
Identify the HS peaks.
Detect the minima points in forward and backward directions for each peak. *(a) Calculate the minimum point* (MP_{FD}) *in forward direction:*

$$\left.\begin{aligned}\left[\frac{d(sig_{env}(n))}{dn}\right]_{n=i+1} &= 0\\ \left[\frac{d(sig_{env}(n))}{dn}\right]_{n=i+1+\Delta_i} &> 0\\ \left[\frac{d(sig_{env}(n))}{dn}\right]_{n=i+1-\Delta_i} &< 0\end{aligned}\right\} \quad (1)$$

(b) Calculate the minimum point (MP_{BD}) *in backward direction:*

$$\left.\begin{aligned}\left[\frac{d(sig_{env}(n))}{dn}\right]_{n=i-1} &= 0\\ \left[\frac{d(sig_{env}(n))}{dn}\right]_{n=i-1+\Delta_i} &> 0\\ \left[\frac{d(sig_{env}(n))}{dn}\right]_{n=i-1-\Delta_i} &< 0\end{aligned}\right\} \quad (2)$$

where i *is the position of HS peak.*
Estimate the boundary B_{HP} *of HS peak.*

$$R(p) = MP_{FD}(p) - MP_{BD}(p) \quad (3)$$

$$B_{HP}(p) = MP_{BD}(\mathrm{p}) + \mathrm{R(p)} \quad (4)$$

where p *is the number of HS peak in the LS signal.*

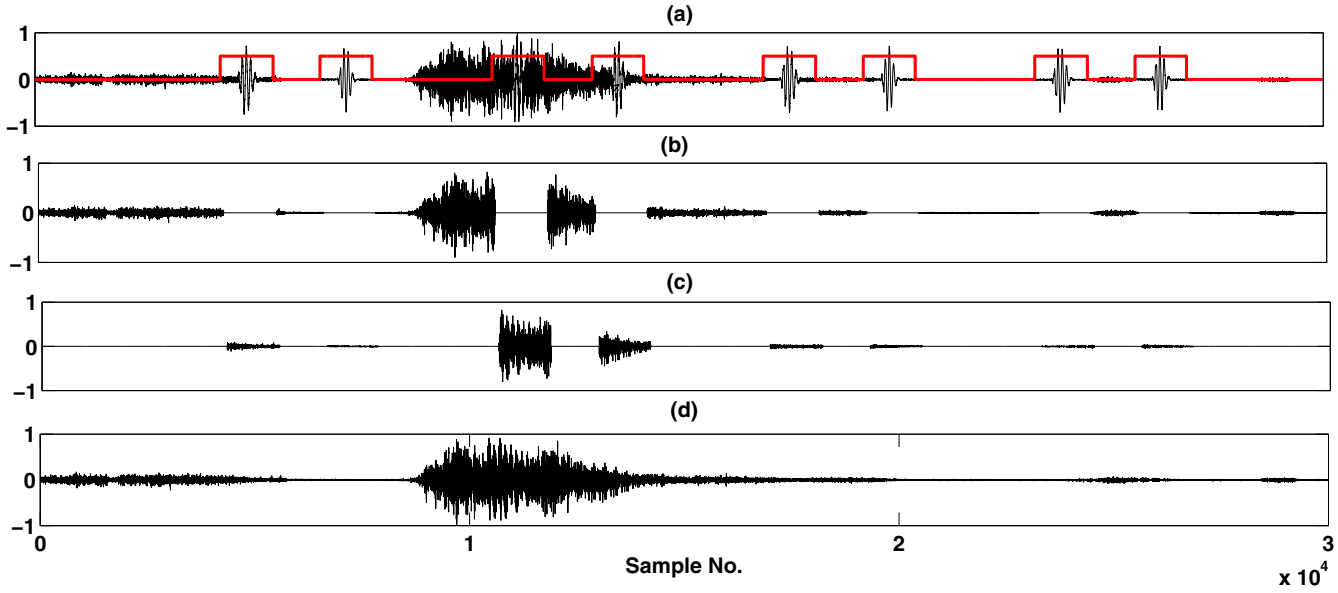

Fig. 4 – (a) A typical example of a HS corrupted LS signal and its associated HS-included segments, (b) waveform of the resultant signal originated after removal of HS-included segments, (c) waveform of the predicted LS signal correspond to created gaps and (d) waveform of the reconstructed LS signal.

coordinates of the boundary of HS corrupted segment corresponding to $m-th$ gap are X_{SP}^{mhsb} and X_{EP}^{mhsb}, respectively. The length of the $m-th$ gap is denoted by L_{gap}^{m} and calculated as follows:

$$L_{gap}^{m} = X_{EP}^{mhsb} - X_{SP}^{mhsb} \tag{5}$$

The length of the created gaps is calculated using Algorithm 3.

Step 2: Estimate the LS values corresponding to the created gap: In this step, the missing values of LS signal corresponding to a created gap are estimated using the transformed domain information of its neighboring samples. In this work, the transformed domain information is obtained by employing an FFT technique. Before doing the FFT operation, the created gap is subdivided into a number of subparts by the following equation.

$$N_{SS} = \left\lceil \frac{L_{gap}}{256} \right\rceil \tag{6}$$

where N_{SS} is the total number of sub-segments. In this work, 256 point FFT and IFFT operation was adopted for prediction of missing LS signals because it gives better result compared to others. It is experimentally observed that subsequent of samples greater than 256 (suppose 512) gives poor result because of high prediction error, due to generation of insufficient number of segments (No. of segments = intervals of HS component × sampling frequency ÷ 512 = 150 ms × 8000 ÷ 512 = 1200 ÷ 512 = 3). On the other hand, subsequent of sample value less than 256 (suppose 128) gives high computational complexity because of generation of many number of subsequent corresponding to gap (1200 ÷ 128 = 10). However, accuracy is more or less same for both cases. In order to estimate LS sample corresponding to each sub-segment, we consider the following criteria:

Algorithm 3: Calculate L_{gap}

Require: $j = 1, k = 1, Y_i^{hsb} = [y_1, y_2, ..., y_N]$ {$y_{i=1,2,...N}$ is the samples values of the HS boundary sequence.}
for $i = 1$ **to** N **do**
  if $Y_i^{hsb} = 0$ & $Y_{i+1}^{hsb} \neq 0$ **then**
    $X_{SP}^{hsb}(j) \leftarrow i + 1$
    $j \leftarrow j + 1$
  end if
  if $Y_i^{hsb} \neq 0$ & $Y_{i+1}^{hsb} = 0$ **then**
    $X_{EP}^{hsb}(k) \leftarrow i$
    $k \leftarrow k + 1$
  end if
end for
for $p = [1, 2, ..., M]$ {M is the total number of starting or end points.} **do**
  $L_{gap}(p) = X_{EP}^{hsb}(p) - X_{SP}^{hsb}(p)$
end for

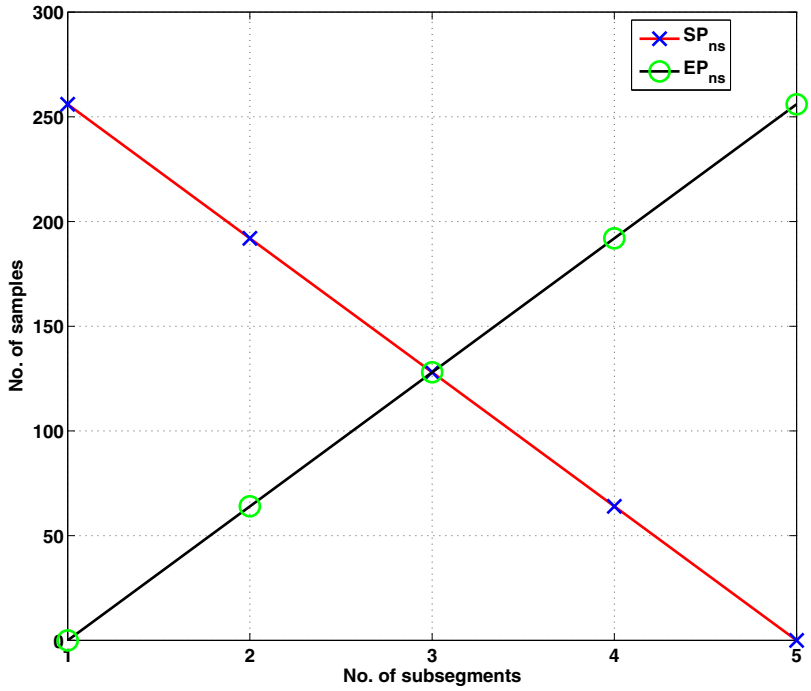

Fig. 5 – The variation of samples employed for prediction of missing LS values corresponding to a typical created gap having 5 subsegments.

Criterion 1: The first sub-segment is very close to the starting point of the created gap and far away from its end point. As the end point is far away from the subsegment, its corresponding missing LS values will be more similar to the neighboring samples of the starting point. Hence, the LS samples corresponding to the first subsegment are predicted using only the FFT values of the starting point neighboring samples (SP_{ns}) of the gap.

Criterion 2: The sub-segments which are lying in between the starting and end point of the gap carry information of both the starting and end point neighboring samples. The LS samples corresponding to these sub-segments are predicted using FFT values of the starting and end point neighboring samples of the gap.

Criterion 3: The last sub-segment is very near to the end point and far away from the starting point of the gap. Hence, LS samples corresponding to the last sub-segment will be more similar to the neighboring samples of the end point. In this case, the missing LS values are estimated using only the FFT values of the end point neighboring samples (EP_{ns}) of the gap.

The variation of samples which are used to predict the missing LS values of a gap is shown in Fig. 5. The steps involved in estimating the missing LS values are explained in details in Algorithm 4.

Algorithm 4: Estimate the missing values correspond to L_{gap}

Require: $sig^i_{res} = [y^1_{res}, y^2_{res}, ..., y^N_{res}]$, $L^k_{gap} = [L^1_{gap}, L^2_{gap}, ..., L^P_{gap}]$ $\{i = 1, 2, ...N$ is the samples values of the resultant signal and P is the total number of created gap.$\}$

for $i = 1$ **to** P **do**

$SP_{ns} = \mathscr{F}(sig_{res}((X_{SP}(i) - 256) : (X_{SP}(i) - 1)), 256)$\{Calculation of FFT values of samples near to the start point of the gap.\}

$EP_{ns} = \mathscr{F}(sig_{res}((X_{EP}(i) + 1) : (X_{EP}(i) + 256)), 256)$\{Calculation of FFT values of samples near to the end point of the gap.\}

for $j = 1$ **to** N_{SS} **do**

$((X_{SP}(i) + (j-1) \times 256) : X_{SP}(i) + (j \times 256 - 1)) =$
$\mathscr{F}^{-1}(((1 - ((j-1) \div (N_{SS} - 1))) \times SP_{ns}) + ((((j-1) \div (N_{SS} - 1)) \times EP_{ns}), 256)$\{Estimation of missing values correspond to each subsegment of the gap and time domain conversion of samples.\}

end for

end for

3.4. Denoising of LS signal corrupted with HS noise

In this stage of the developed framework, some operations are performed in order to obtain LS signal free from HS noise. The phases associated with this enhancement stage are as follows:

3.4.1. Segmentation of HS free LS portions in the IMF

It is experimentally noticed that IMF carries information of both HS and LS signals. In this step, HS free (HF) regions associated with IMF are identified by removing the HS included (HI) segments from them. This operation is done individually for each IMF by the following Eq. (7)

$$HF_i(n) = IMF_i(n) - HI_i(n) \tag{7}$$

where i indicates the particular IMF, i = 1, 2, …, m, $HI_i(n)$ stands for HS-included portions and $HF_i(n)$ for HS-free portion of $IMF_i(n)$.

3.4.2. Computation of resultant signal

The resultant signal $sig_{res}(n)$ free of HS noise and associated with several gaps is computed by combining linearly the segmented LS portations for all IMFs and it is depicted in Fig. 4(b).

$$sig_{res}(n) = \sum_{i=1}^{m} HF_i(n) \tag{8}$$

3.4.3. Logical operation with estimated LS samples

The time domain LS signal is reconstructed by a linear additive operation between the resultant signal $sig_{res}(n)$ and the predicted LS ($LS_p(n)$) signal obtained using FFT based algorithm. Before performing the summing operation, it is necessary to convert the predicted LS samples from FFT domain into time domain using an inverse FFT technique. However, the predicted LS samples are overlapped with the resultant signal $sig_{res}(n)$ samples near the end point of a gap due to 256 point FFT operation. This leads to an inaccurate prediction of the result. In this work, we solve this problem by discarding the overlapped predicted samples from the resultant signal by a logical XOR operation between the resultant signal $sig_{res}(n)$ and the predicted LS ($LS_p(n)$) signal. Hence, the non-overlapped predicted LS can be obtained by the following logical operation:

$$sig_{res}(n) \oplus LS_p(n) = sig_{res}(n)\overline{LS_p(n)} + \overline{sig_{res}(n)}LS_p(n) \tag{9}$$

where ($\oplus$) is a logical operator. The truth table of the operation $sig_{res}(n) \oplus LS_p(n)$ is given in Table 1. The first and second conditions of the truth table are never satisfied due to the non-zero value of the estimated LS samples. Hence, the third and fourth conditions are necessary and sufficient conditions for the operation and truth table modified according to the conditions is presented in Table 2. In this logical process, the third condition determines the non-overlapped LS samples and the fourth condition discards the overlapped LS samples. The steps involved in the operation are explained in Algorithm 2. The waveform of the predicted LS corresponding to created gaps is shown in Fig. 4(c).

Table 1 – Truth table for XOR logical operation between the resultant signal ($sig_{res}(n)$) and the predicted LS ($LS_p(n)$) signal.

Input		Output
$LS_p(n)$	$sig_{res}(n)$	
0	0	0
0	1	1
1	0	1
1	1	0

"1" stands for presence of sample value and "0" stands for absence of sample value.

Table 2 – Modified truth table for XOR logical operation between the resultant signal ($sig_{res}(n)$) and the predicted LS ($LS_p(n)$) signal.

Input		Output
$LS_p(n)$	$sig_{res}(n)$	
1	0	1
1	1	0

"1" stands for presence of sample value and "0" stands for absence of sample value.

3.4.4. Reconstruction of LS signal

Add up the resultant signal $sig_{res}(n)$ to the output of Step 3, and as a result, obtain the reconstructed LS signal without HS interference. A typical mixed signal associated with HS boundary and reconstructed LS signal along with its comprising resultant signal and predicted signal are shown in Fig. 4. The reconstructed LS signals contain information that help the doctors or machine intelligence system to make a correct decision regarding the lung diseases.

Algorithm 5: Eliminate unwanted predicted LS samples

Require: $j = 1, k = 1, Y_i^{hsb} = [y_1, y_2, ..., y_N]$ {$y_{i=1,2,...N}$ is the samples values of the HS boundary sequence.}
  for $i = 1$ **to** N **do**
    if $Y_i^{hsb} \neq 0$ & $sig_{res}^i = 0$ **then**
      $LS_p(i) = Y_i^{hsb}$
    end if
  end for

4. Experimental data sets and implementation issues

4.1. Data acquisition

The lung sound signals are recorded from the test subjects using a single channel stethoscope based data acquisition system (DAS). The DAS has been constructed by making a circuit using active devices and passive elements which is fitted to a stethoscope device through a condenser type microphone transducer. The primary functional blocks of the data acquisition system include a stethoscope tool, an acoustic-to-electric transducer, an embedded circuit and an analog to digital converter. The embedded circuit consists of a low-noise pre amplifier, low pass active filters and some passive elements which include few resistors, several bypass and coupling capacitors. The active devices are powered through a dual polarity 12V supply.

An acoustic stethoscope has been used to transmit sound produced from the lungs via chest piece and an air-filled hollow tube. Finally, the sound reaches into a DC-biased condenser microphone transducer which is placed inside the tube with special care to reduce the noise level.

4.2. Database for the studies and experimental procedures

The lung sounds data are recorded from healthy and unhealthy subjects. The pathological subjects are associated with different types of lung diseases such as chronic obstructive pulmonary diseases (COPDs), diffuse interstitial lung disease (DILD) and asthma. The pathological LS are recorded from 20 male and 8 female subjects and the normal LS are recorded from 5 male healthy subjects. The lung sounds are recorded from different auscultation locations over the body surface (e.g., left intercostals spaces, right intercostals spaces and suprasternal notch location) of the patients in the sitting position and under relaxed mood conditions. The recordings are not associated with any particular age group. The data are recorded in 16 bit, PCM, mono audio format at sampling frequency of 8 kHz and stored as *.wav files.

4.3. Simulated data

In this study, simulated mixed sound data are produced by convoluting the lung sound signal with heart sound signal based on a mixture producing technique [54]. The corrupted lung sound data are synthesized by imposing the filtered lung sound components $FS_{LS}(t)$ onto the filtered heart sound $FS_{HS}(t)$ as given next.

$$Sim_{CM}(t) = FS_{HS}(t) + FS_{LS}(t) \tag{10}$$

$$FS_{HS}(t) = \sum_{i=0}^{3} b_i S_{HS}(t-i) \tag{11}$$

$$FS_{LS}(t) = \sum_{j=0}^{3} a_j S_{LS}(t-j) \tag{12}$$

where b_i and a_j are the vectors of heart sound and lung sound filter coefficients, respectively. These are four dimensional vectors, i.e., $\mathbf{b}_i = [b_{i0}, b_{i1}, b_{i2}, b_{i3}]^T$ and $\mathbf{a}_j = [a_{j0}, a_{j1}, a_{j2}, a_{j3}]^T$. The heart sound filter coefficient vector $\mathbf{b}_i$ is normalized to one, i.e., $\|\mathbf{b}_i\| = 1$. These filter coefficients are generated randomly.

The low, medium and high flow rates mixed signal are produced by varying the amplitude ratios of the lung and heart sound signals. The value of the norm of the lung sound filter coefficients vector a_j varies according to the breathing flow rates [45].

4.4. Implementation platform

In this study, an ACER-PC with 3.29 GHz Intel core 2 quad CPU and 3.49 GB of RAM has been used to implement the algorithm. All the experiments are conducted in MATLAB environment (R2008a, The Mathworks, Inc., Natick, MA).

5. Results and discussion

The performance of the proposed method is evaluated by auditory test and visual inspection of the results. The visual inspection analysis includes temporal, spectral and tempo-spectral domain comparisons of the results. In addition to the subjective analysis, an objective analysis of the results has been done by comparing the proposed method with a baseline method [38] in terms of average power difference in power spectral density (PSD) between the original LS and reconstructed LS signals. The PSD difference results are computed over several frequency bands using Welch method [56]. Apart from the audio and visual analysis, the efficacy of proposed method is evaluated statistically in terms of cross correlation index (CCI), signal to deviation ratio (SDR), and normalized maximum amplitude error (NMAE). The experiments are conducted with simulated HS corrupted LS data and recoded HS corrupted LS data. The simulated data used in this work are of two types: normal and abnormal. The experiments are carried out several times with different signals at different flow rates and various SNR levels.

5.1. Qualitative analysis of the results

5.1.1. Auditory test

A subjective test by experienced and skilled pulmonologist has been performed on the reconstructed LS signals without HS interference. Listening to the reconstructed LS signals confirmed that the HS interference is completely removed. Hence, the proposed method is able to produce HS-free LS signals with high sound quality.

5.1.2. Visual inspection of the mixed and reconstructed lung sound signals

Instead of the auditory test, a visual analysis of the results is performed. In this work, time domain, frequency domain and combination of these two domains have been taken under

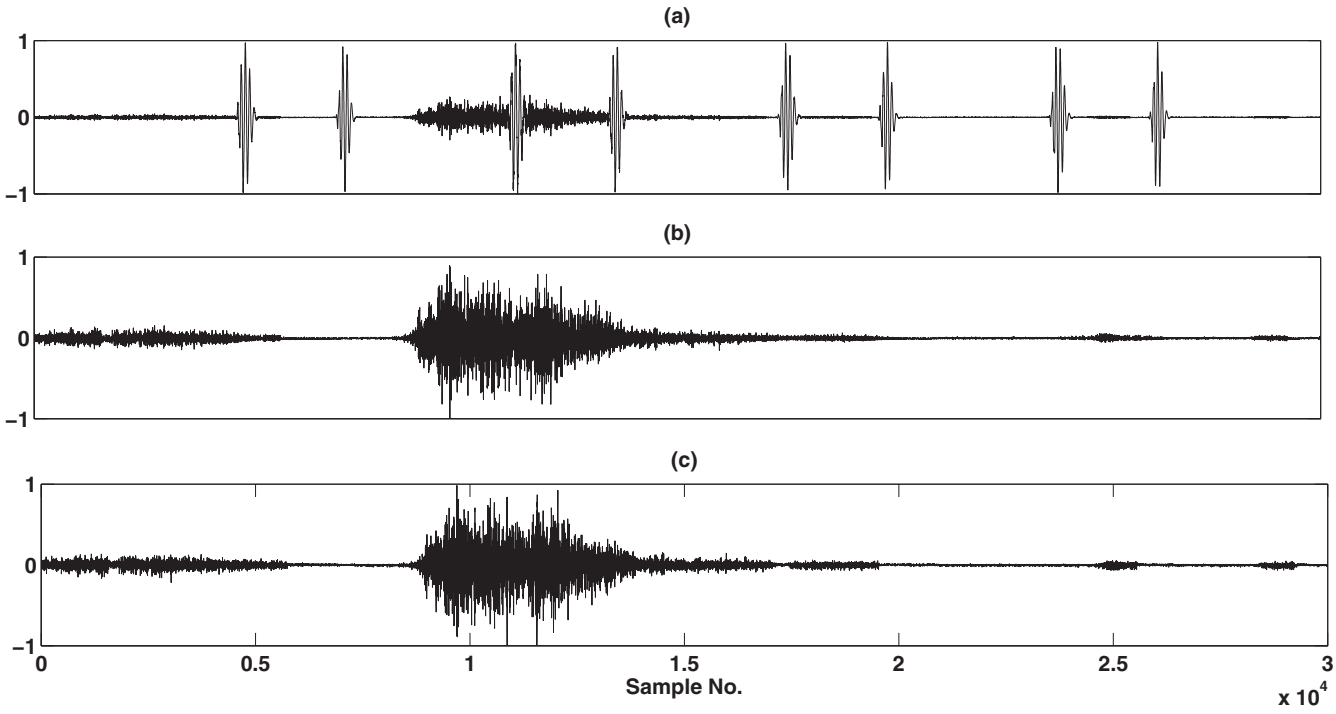

Fig. 6 – Reduction of HS interference from corrupted normal LS signal at low flow. (a) Waveform of a HS corrupted LS record, (b) waveform of the reconstructed HS-free LS signal and (c) waveform of the original LS signal free from HS interference was employed to form simulated mixed signal of HS and LS.

consideration in order to visualize the similarity between the original HS free LS signal and reconstructed LS signal.

5.1.2.1. *Time domain comparison of the results*. The waveform analysis of the results has been done for three types of mixed signal: a simulated mixture of normal LS and HS, a simulated mixture of abnormal LS and HS and a real recorded mixture of LS and HS. The time domain representations of the HS corrupted normal LS signal, reconstructed normal LS signal free of HS interference, and original HS-free normal LS signal are shown in Fig. 6. Fig. 7 displays the waveforms of the HS corrupted abnormal LS signal, reconstructed HS free abnormal LS signal, and original abnormal LS signal free of HS interference. The real recoded HS contaminated LS signal and its corresponding reconstructed LS signal are shown in Fig. 8. These figures show that reconstructed LS signal closely resembles the original LS signal. However, the degree of similarity between reconstructed LS signal and original LS signal is greater for normal LS signal than abnormal LS signal. Because, HS localization algorithm gives more false positive error (FPE) and detection error rate (DER) for abnormal LS signal. By time domain analysis of the results, it is evident that the method can reduce the HS interference from LS signal.

5.1.2.2. *Frequency domain comparison of the results*. Besides the time domain inspection, performance of the method is verified by comparing the power spectral densities (PSDs) of the LS signals with and without HS interference with that of the reconstructed LS signal. In this work, the PSD is calculated by Welch method. Here, discrete Fourier transform of the Gaussian windowed segment of 200 ms length with 50% overlap between successive segments is computed using FFT algorithm. For an effective HS removal method, the PSD of the reconstructed LS signal should coincide or be close to that of the original HS-free LS signal. Fig. 9 shows the PSDs of the mixed signal, reconstructed LS signals obtained by the proposed method and original LS signal, respectively for simulated normal LS data. Fig. 10 shows the PSDs of the mixed signal, reconstructed LS signal obtained by the proposed method and original LS signal, respectively for simulated abnormal LS data. These figures show that PSD of the reconstructed HS free LS signal is close to the PSD of the original LS signal free of HS interference. The PSD comparisons corroborate the proposed method can efficiently reduce the HS interference from the desired LS signals.

5.1.2.3. *Time-frequency domain or spectrogram comparison of the results*. The performance of the developed method is also evaluated by subjective analysis of the spectrograms of noisy LS signals, reconstructed pure LS signals and original LS signal. Fig. 11 illustrates the spectrogram of mixed signal, reconstructed LS signal and original LS signal for simulated normal data. Fig. 12 displays the spectrograms of mixed signal, reconstructed LS signal and original LS signal for simulated abnormal data. The spectrograms of mixed signal and reconstructed LS signals for real time recorded data are shown in Fig. 13. By visually inspecting the spectrograms of the simulated and real time recorded signals, it is evident that the method successfully removes the HS interference from LS signal.

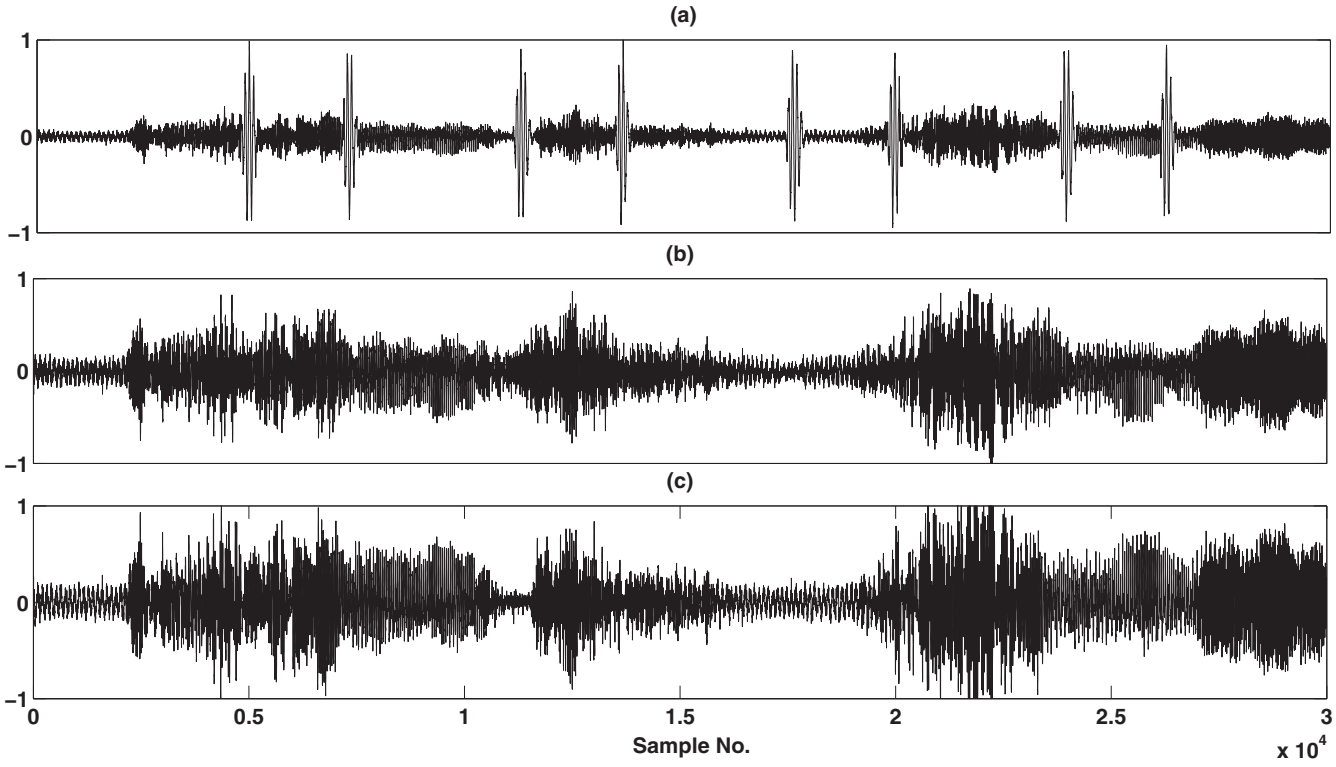

Fig. 7 – Reduction of HS interference from corrupted abnormal LS signal at low flow. (a) Waveform of a HS corrupted LS record, (b) waveform of the reconstructed HS-free LS signal and (c) waveform of the original LS signal free from HS interference was employed to form simulated mixed signal of HS and LS.

5.2. *Quantitative analysis of the results*

In addition to the subjective test, the performance of the proposed method is also analyzed quantitatively. The quantitative evaluation of the results is done by computing the average power difference between the original LS signal free of HS components and reconstructed LS signal free of HS interference. The average power differences are calculated over four frequency bands: 20–70, 70–120, 120–170 and 170–300 Hz, as discussed in [38]. The superiority of the proposed method is validated by comparing it with a baseline method [38]. The database mentioned in subsection IV-D has been used in order to perform quantitative comparison between the proposed method and existing method [38]. Results obtained using the proposed method and baseline method for different flow rates signals are presented in Table 3, Table 4 and Table 5, respectively. The tables show that the performance of the proposed method is higher than that of the existing method at different flow rates. The baseline method recovers the HS-free LS signal from the corrupted LS record using periodicity of the HS signal. However, the cyclic atoms corresponding to HS component may not be detected accurately from the atoms of the mixed signal due to several reasons: influence of surrounding noise, manmade artifacts, data recording and processing instruments disturbances, variation of LS intensity at different flow rates and implementation of nonadaptive kernel based

Table 4 – Experimental results for simulated HS corrupted normal LS signal at medium flow rate.

Frequency bands (Hz)	Average power difference (dB)	
	Proposed method	Baseline method
20–70	1.7694 ± 1.6862	4.4358 ± 0.8737
70–120	1.1012 ± 0.7157	1.5808 ± 0.4543
120–170	0.7714 ± 0.7848	0.8653 ± 0.8189
170–300	0.3887 ± 0.2425	0.7024 ± 0.5940

Table 3 – Experimental results for simulated HS corrupted normal LS signal at low flow rate.

Frequency bands (Hz)	Average power difference (dB)	
	Proposed method	Baseline method
20–70	1.0734 ± 0.4244	2.2708 ± 0.5564
70–120	0.5161 ± 0.2743	1.1557 ± 0.1170
120–170	0.4152 ± 0.2529	0.7990 ± 0.2565
170–300	0.2267 ± 0.1902	0.5057 ± 0.3452

Table 5 – Experimental results for simulated HS corrupted normal LS signal at high flow rate.

Frequency bands (Hz)	Average power difference (dB)	
	Proposed method	Baseline method
20–70	3.4615 ± 1.2043	7.1703 ± 1.2592
70–120	2.2721 ± 0.5449	3.6747 ± 1.6377
120–170	1.4536 ± 0.7100	2.1551 ± 1.7798
170–300	0.9810 ± 0.8712	1.4066 ± 1.5609

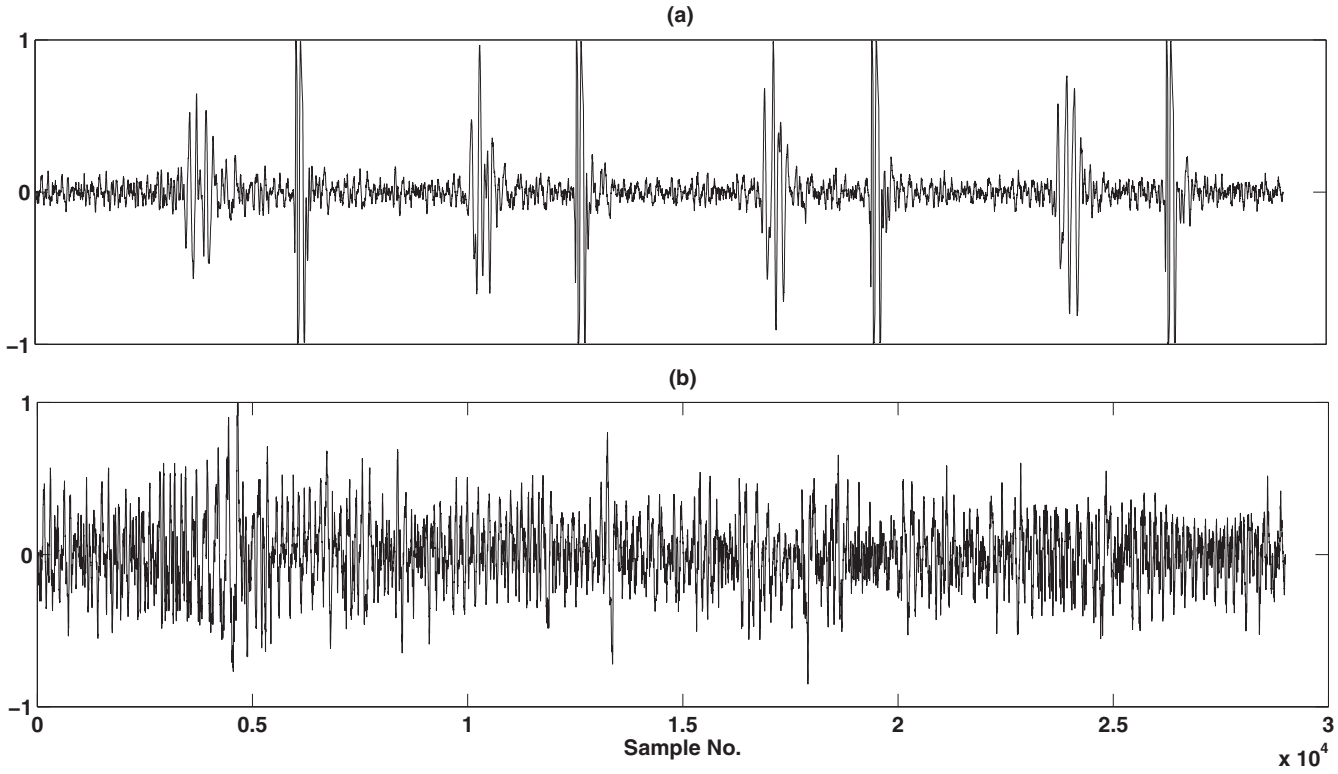

Fig. 8 – Reduction of HS interference from a real time recorded LS signal at low flow. (a) Waveform of a real recorded HS corrupted LS signal and (b) waveform of the reconstructed HS-free LS signal.

short time Fourier transform (STFT) for decomposition of the corrupted LS signal into time-frequency atoms. In this work, an adaptive kernel based EMD technique is used to decompose the corrupted LS signal into its embedded components and surrounding noise is reduced by recording the lung sounds in a quiet environment. On the other hand, the instrumental disturbances are removed with a first order differentiation algorithm [57] [58], and manmade artifacts are suppressed by

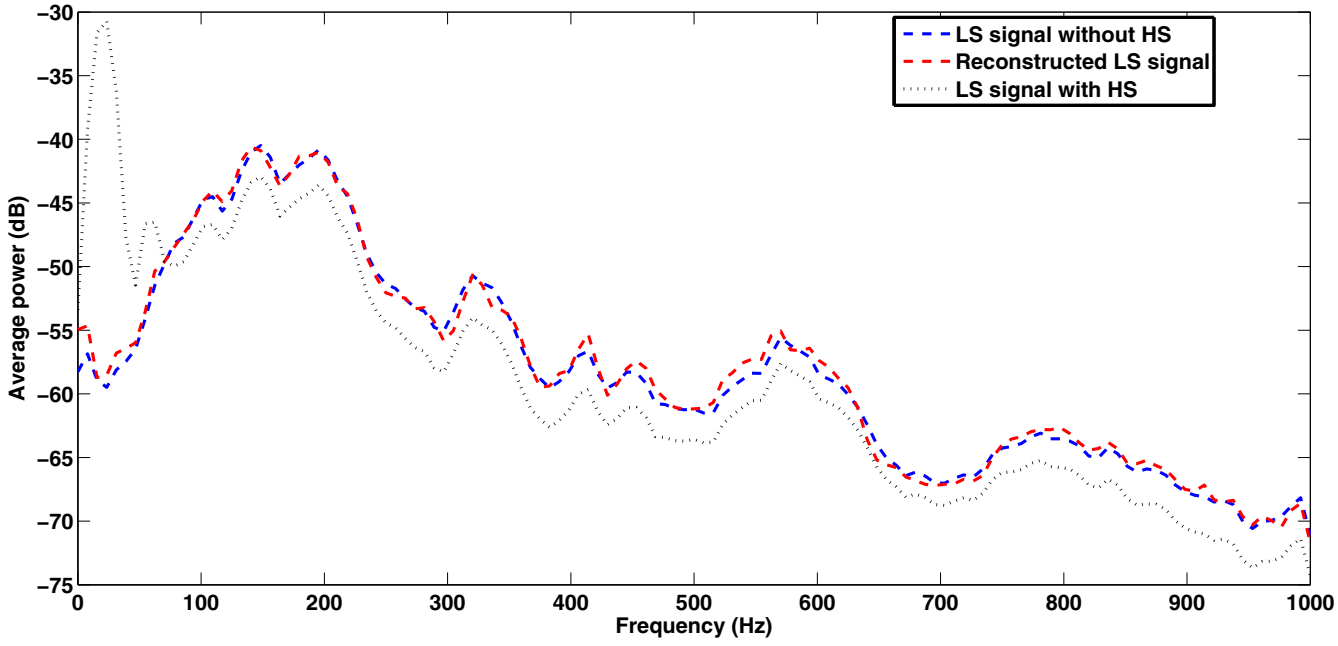

Fig. 9 – PSDs of the mixed signal, reconstructed normal LS signal using our proposed method, and original HS-free normal LS signal.

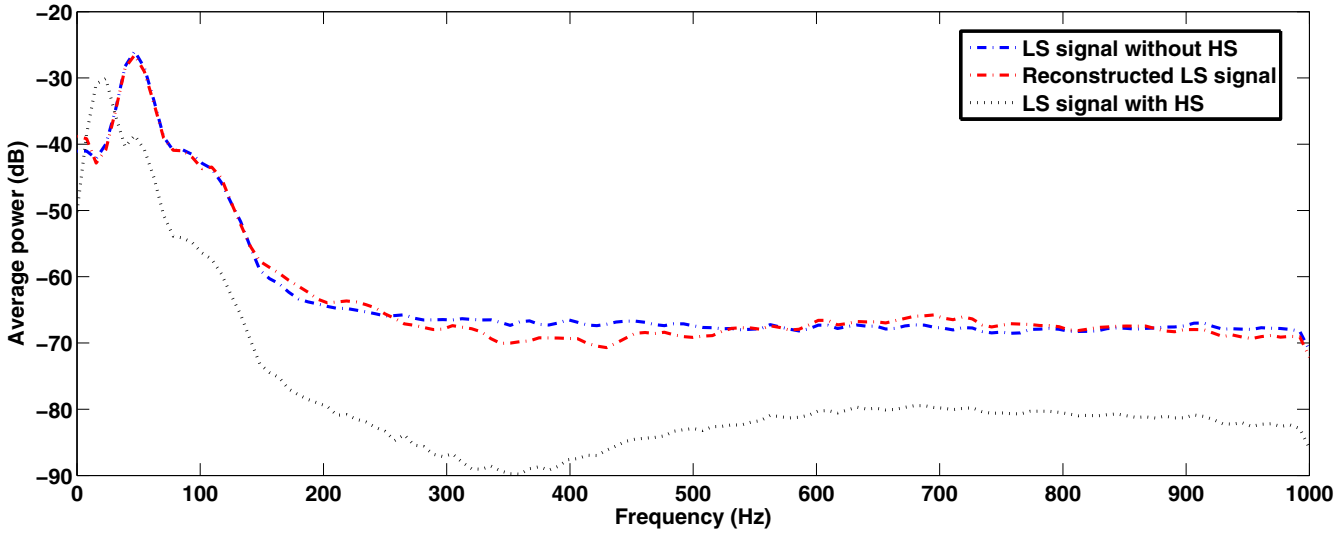

Fig. 10 – PSDs of the mixed signal, reconstructed abnormal LS signal using our proposed method, and original HS-free abnormal LS signal.

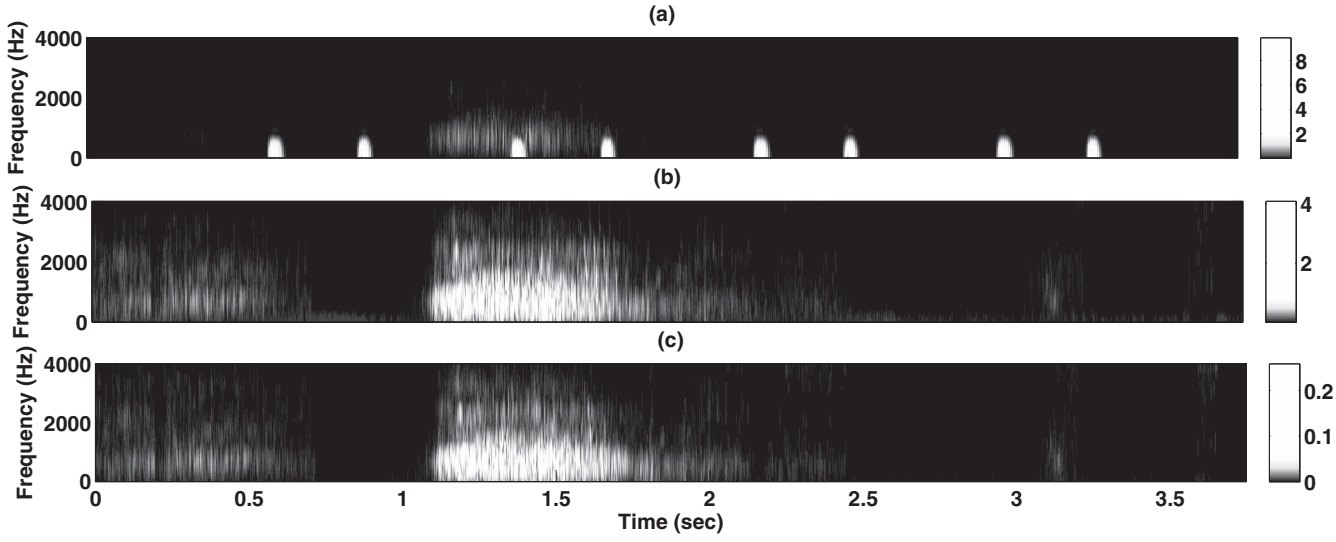

Fig. 11 – Spectrograms of the mixed signal (Fig. 11(a)), the reconstructed normal LS signal (Fig. 11(b)) and original normal LS signal free from HS signal (Fig. 11(c)).

placing the stethoscope in a proper way over the recording positions of the subject. The effect of flow rate is minimized by filtering the corrupted LS signal by applying a Butterworth filter of length 10 and cutoff frequency 150 Hz. Moreover, the developed method is faster than the baseline method because the later one involves various time consuming operations such as atom decomposition, phase detection and selection of cyclic atoms. The comparison results for time consumption of the proposed method and the baseline method at different flow rates are presented in Table 6.

5.3. *Statistical evaluation of the results*

In addition to qualitative and quantitative analysis of the results, performance of the proposed method has been measured using different statistical evaluation metrics such as cross correlation index (CCI), signal to deviation ratio (SDR), and normalized maximum amplitude error (NMAE). These statistical parameters are calculated at different signal to noise ratio (SNR) values

Table 6 – Comparison of execution time between proposed method and baseline method.

Types of flows	Execution time (sec)	
	Proposed method	Baseline method
Low	10.84 ± 0.95	238.14 ± 47.41
Medium	10.99 ± 1.21	711.92 ± 215.50
High	11.16 ± 1.52	1284.86 ± 297.56

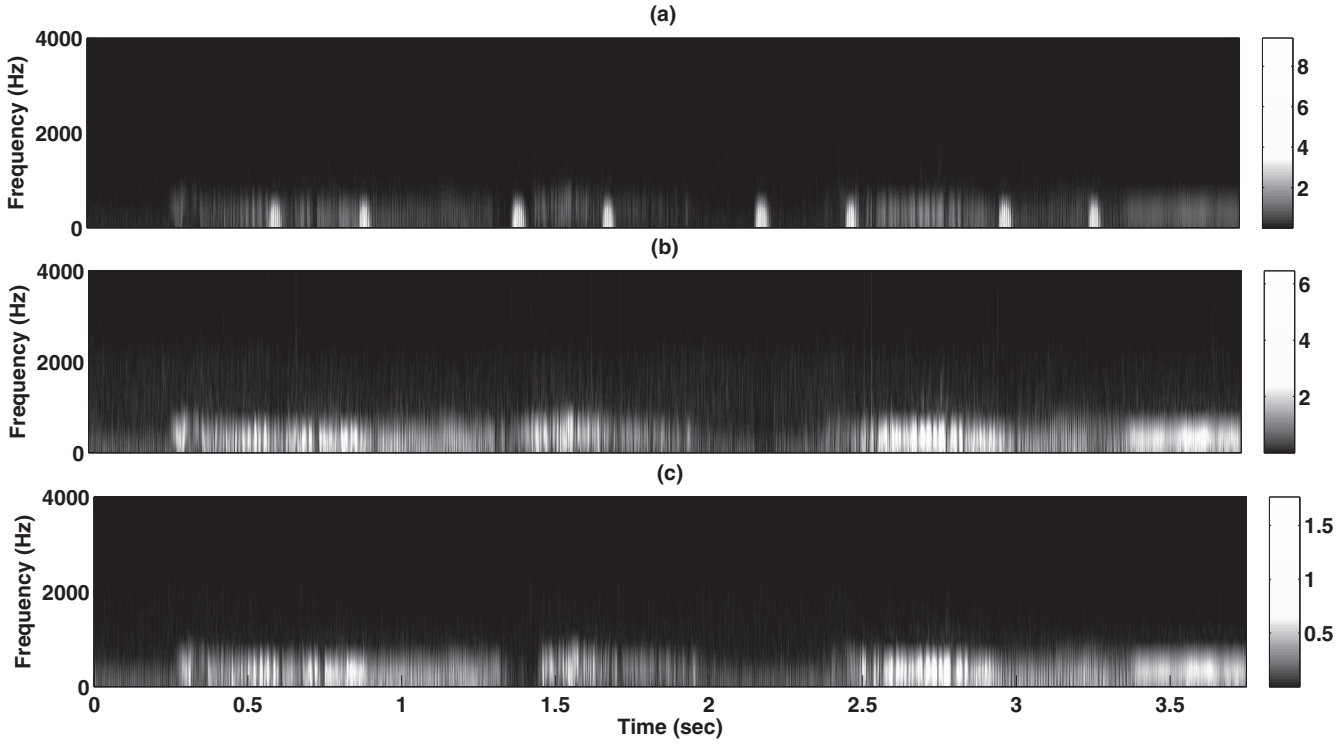

Fig. 12 – Spectrograms of the mixed signal (Fig. 12(a)), reconstructed abnormal LS signal (Fig. 12(b)) and original abnormal LS signal free from HS signal (Fig. 12(c)).

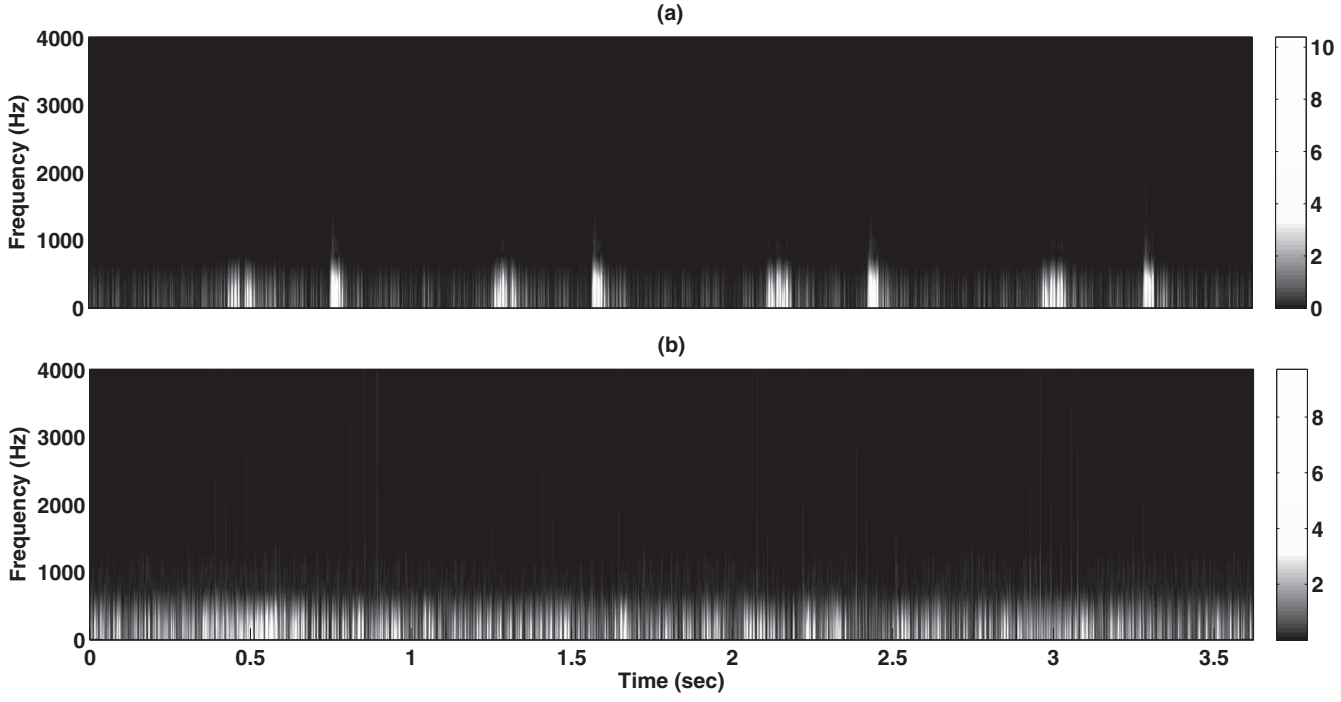

Fig. 13 – Spectrograms of the real time recorded mixed signal (Fig. 13(a)) and the reconstructed LS signal (Fig. 13(b)).

Table 7 – Statistical evaluation of the results.

SNR (dB)	CCI		SDR (dB)		NAME	
	Proposed method	Baseline method	Proposed method	Baseline method	Proposed method	Baseline method
8	0.9507	0.5369	10.0471	7.6518	18.82	22.16
6	0.9505	0.5218	10.0222	7.1652	19.34	24.37
4	0.9502	0.4523	9.9026	6.5193	22.09	25.69
2	0.9498	0.4321	9.9733	6.0247	25.88	26.91
0	0.9488	0.4258	9.8262	5.1728	26.94	28.12
–2	0.9484	0.4079	9.7902	4.9456	27.13	29.74
–4	0.9481	0.3792	9.7068	4.2673	27.98	30.28
–6	0.9465	0.3572	9.6230	3.7319	28.45	30.88
–8	0.9388	0.3138	9.4640	3.1629	29.57	31.07

in order to measure the efficacy of proposed method. The evaluation metrics are defined by the following equations.

$$CCI = \frac{\sum_{l=0}^{N-1}[LS(l) - mean(LS(l))].[RLS(l) - mean(RLS(l))]}{\sqrt{\sum_{l=0}^{N-1}[LS(l) - mean(LS(l))]^2}.\sqrt{\sum_{l=0}^{N-1}[RLS(l) - mean(RLS(l))]^2}} \tag{13}$$

$$SDR = 10\log\left[\frac{\sum_{l=0}^{N-1}[LS(l)]^2}{\sum_{l=0}^{N-1}[RLS(l) - LS(l)]^2}\right] \tag{14}$$

$$NMAE = \frac{max|LS(l) - RLS(l)|}{max(LS(l)) - min(RLS(l))} \tag{15}$$

where LS represents the original lung sound signal and RLS is the reconstructed lung sound signal and l indicates sample of the signal, its maximum value is N-1.

The experiments are conducted several times with various signals and noisy components in order to justify reliability and robustness of the results. These metrics generally measure the similarity between original LS and reconstructed LS signal in terms of matching score grading and deviation or distortion ratio of individual samples. The statistics of enhancement technique is given in Table 7. The table shows that proposed method gives better results compared to baseline method for different SNR levels. For example, at SNR value of 0 dB the CCI is 0.9488, SDR is 9.8262, and NMAE is 26.94 for proposed method and baseline method gives CCI of 0.4258, SDR of 5.1728, and NAME of 28.12. It is observed from the table that normalized maximum amplitude error increases in decreasing of SNR levels and on the other hand, cross correlation index and signal to deviation ratio decreases correspondingly. This happens because of the inaccurate estimation of missing LS samples corresponding to gap. The prediction algorithm gives erroneous value due to presence of noisy component prominently at low SNR value. The visual analysis of the statistical results is represented in Fig. 14 and Fig. 15 for SNR values 8 dB and 6 dB, respectively.

6. Conclusion

In this paper, a new method has been proposed based on EMD approach and missing value prediction algorithm for cancellation of HS interference from LS record. The EMD process provides a way to analyze the signal in more details by decomposing the signal components in terms of IMF components. In this method, the HS-included segments in LS record are identified by Hilbert Heron Algorithm (HHA) [45], and these segments are removed from each IMF component. Thereafter, the missing values of LS signal corresponding to created gap are estimated by an FFT based prediction algorithm. The performance of the proposed method is evaluated through subjective and

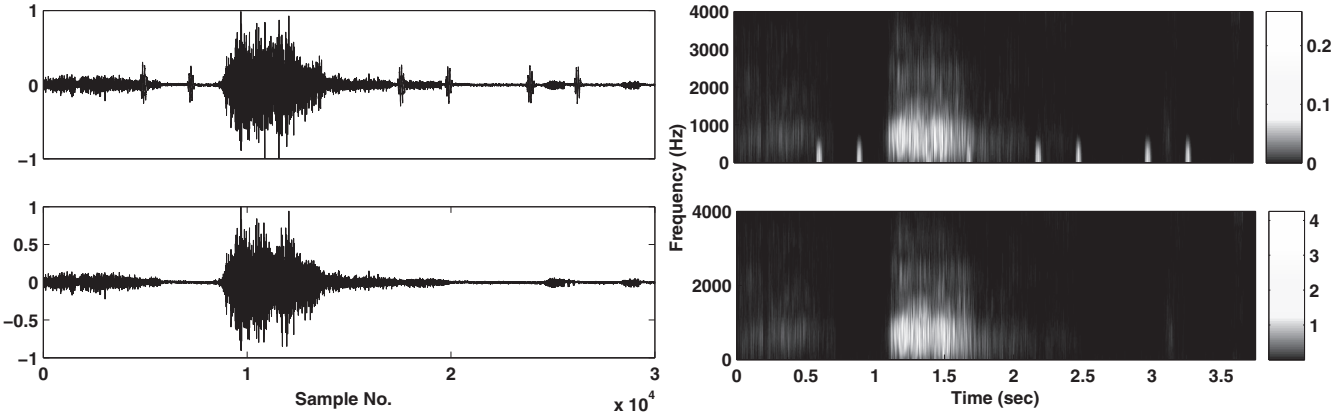

Fig. 14 – The waveforms and spectrograms of mixed signal (top) and reconstructed LS signal (bottom) for SNR 8 dB.

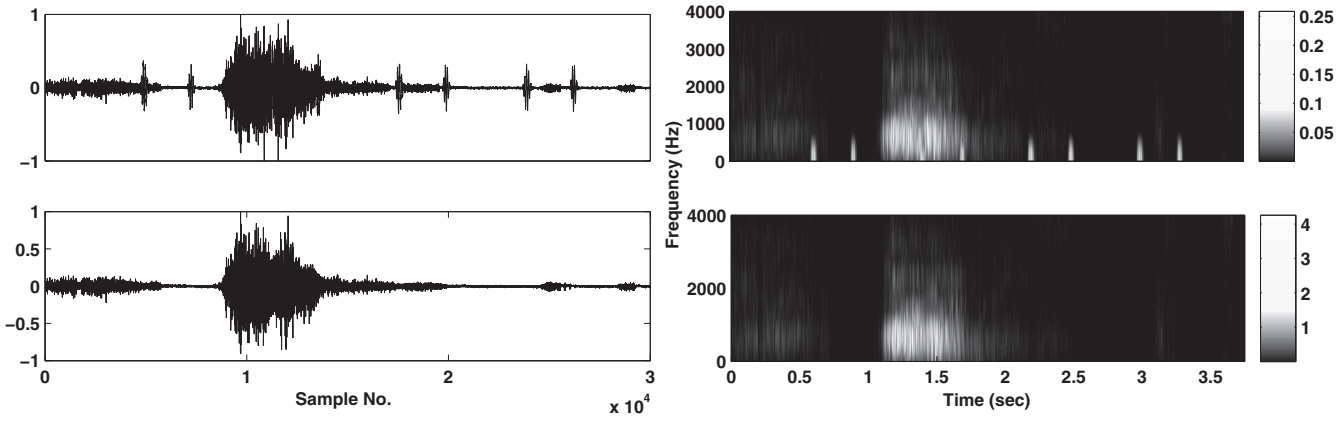

Fig. 15 – The waveforms and spectrograms of mixed signal (top) and reconstructed LS signal (bottom) for SNR 6 dB.

objective analysis of the results. In addition, a comparison test is done with a baseline method [38] in order to validate the effectiveness of the proposed method. The qualitative analysis shows that the method can efficiently reduce HS interference from LS record. The quantitative analysis proves that the proposed method is superior in terms of average power difference, normalized maximum amplitude error, signal to deviation ratio, cross correlation index and execution time. The proposed method may be incorporated into a lung sound analysis system as an important preprocessing step to enhance the quality of the lung sound signal for accurate diagnosis of pulmonary diseases.

Acknowledgment

This work is financially supported by the Institute of Pulmocare and Research of India. The authors would like to thank Dr. Partha Sartahi Bhattacharyya for his cooperation to collect lung sound data and validation.

REFERENCES

[1] P. Forgacs, The functional basis of pulmonary sounds, Chest 73 (3) (1978) 399–405.
[2] W.K. Blake, Mechanics of Flow-Induced Sound and Vibration, Academic Press, Orlando, FL, 1986.
[3] J.C. Hardin, J.L. Patterson Jr., Monitoring the state of the human airways by analysis of respiratory sound, Acta Astronaut. 6 (9) (1979) 1137–1151.
[4] J.G. Webster, Chapter 7, Medical Instrumentation, Application and Design, John Wiley & Sons, Inc., New York, NY, 1998.
[5] M.T. Pourazad, Heart sounds reduction from lung sounds recordings applying signal and image processing techniques in time-frequency domain (M.Sc. thesis), Elect. Comput. Eng. Dept., Univ. Manitoba, Winnipeg, MB Canada, 2004.
[6] D. Balasubramaniam, D. Nedumaran, Efficient computation of phonocardiographic signal analysis in digital signal processor based system, Int. J. Comput. Theory Eng. 2 (2010) 1793–8201.
[7] P.J. Arnott, G.W. Pfeiffer, M.E. Tavel, Spectral analysis of heart sounds: Relationships between some physical characteristics and frequency spectra of first and second heart sounds in normals and hypertensives, J. Biomed. Eng. 6 (2) (1984) 121–128.
[8] Y.-S. Lu, W.-H. Liu, G.-X. Qin, Removal of the heart sound noise from the breath sound, in Proc. IEEE 10th Annual International Conference of the Engineering in Medicine and Biology Society, 1 (1988) 175–176.
[9] L. Cromwell, F.J. Weibell, E.A. Pfeiffer, Biomedical instrumentation and measurements, second ed., PHI Publication, New Delhi, 2002.
[10] R.T.H. Laennec, Invention of the Stethoscope. Acoustics Historical and Philosophical Development, Dowden, Hutchinson and Ross Inc., Stroudsburg, PA, 1962.
[11] A. Kandaswamy, C. Sathish Kumar, R.P. Ramanathan, S. Jayaraman, N. Malmurugan, Neural classification of lung sounds using wavelet coefficients, Comput. Biol. Med. 34 (6) (2004) 523–537.
[12] S.A. Taplidou, L.J. Hadjileontiadis, Wheeze detection based on time-frequency analysis of breath sounds, Comput. Biol. Med. 37 (8) (2007) 1073–1083.
[13] S. Sello, S. Kyung Strambi, G.D. Michele, N. Ambrosino, Respiratory sound analysis in healthy and pathological subjects: a wavelet approach, Biomed. Signal Process. Control 3 (3) (2008) 181–191.
[14] M. Bahoura, Pattern recognition methods applied to respiratory sounds classification into normal and wheeze classes, Comput. Biol. Med. 39 (9) (2009) 824–843.
[15] R.J. Riella, P. Nohama, J.M. Maia, Method for automatic detection of wheezing in lung sounds, Braz. J. Med. Biol. Res. 42 (7) (2009) 674–684.
[16] Z. Wu, N.E. Huang, Ensemble empirical mode decomposition: a noise-assisted data analysis method, Adv. Adap. Data Anal. 1 (2009) 1–41.
[17] R.J. Riella, P. Nohama, J.M. Maia, Methodology for automatic classification of adventitious lung sounds, in Proc. International Conference on Medical Physics and Biomedical Engineering 25 (2010)1392–1395.
[18] G.C. Chang, Y.F. Lai, Performance evaluation and enhancement of lung sound recognition system in two real noisy environments, Comput. Methods Programs Biomed. 97 (2) (2010) 141–150.
[19] S. Charleston-Villalobos, G. Martinez-Hernandez, R. Gonzalez-Camarena, G. Chi-Lem, J.G. Carrillo, T. Aljama-Corrales, Assessment of multichannel lung sounds parameterization for two-class classification in interstitial

lung disease patients, Comput. Biol. Med. 41 (7) (2011) 473–482.
[20] L.E. Ellington, R.H. Gilman, J.M. Tielsch, M. Steinhoff, D. Figueroa, S. Rodriguez, et al., Computerised lung sound analysis to improve the specificity of paediatric pneumonia diagnosis in resource-poor settings: protocol and methods for an observational study, BMJ 2 (1) (2012) 1–7.
[21] D.S. Morillo, A.L. Jiménez, S.A. Moreno, Computer-aided diagnosis of pneumonia in patients with chronic obstructive pulmonary disease, J. Am. Med. Inform. Assoc. 20 (1) (2013) 111–117.
[22] B.A. Reyes, S. Charleston-Villalobos, R. González-Camarena, T. Aljama-Corrales, Assessment of time? Frequency representation techniques for thoracic sounds analysis, Comput. Methods Programs Biomed. 114 (2014) 276–290.
[23] Y.A. Amrulloh, U.R. Abeyratne, V. Swarnkar, R. Triasih, A. Setyati, Automatic cough segmentation from non-contact sound recordings in pediatric wards, Biomed. Signal Process. Control 21 (2015) 126–136.
[24] R. Naves, B.H. Barbosa, D.D. Ferreira, Classification of lung sounds using higher-order statistics: a divide-and-conquer approach, Comput. Methods Programs Biomed. 129 (2016) 12–20.
[25] N. Gavriely, M. Nissan, A.H. Rubin, D.W. Cugell, Spectral characteristics of chest wall breath sounds in normal subjects, Thorax 50 (12) (1995) 1292–1300.
[26] V.K. Iyer, P.A. Ramamoorthy, H. Fan, Y. Ploysongsang, Reduction of heart sounds from lung sounds by adaptive filtering, IEEE Trans. Biomed. Eng. 12 (33) (1986) 1141–1148.
[27] M. Kompis, E. Russi, Adaptive heart-noise reduction of lung sounds recorded by a single microphone, in Proc. IEEE 14th Annual International Conference of the Engineering in Medicine and Biology Society, 2 (1992)691–692.
[28] L.J. Hadjileontiadis, S.M. Panas, Adaptive reduction of heart sounds from lung sounds using fourth-order statistics, IEEE Trans. Biomed. Eng. 44 (7) (1997) 642–648.
[29] J. Gnitecki, Z. Moussavi, H. Pasterkamp, Recursive least squares adaptive noise cancellation filtering for heart sound reduction in lung sounds recordings, in Proc. IEEE 25th Annual International Conference of the Engineering in Medicine and Biology Society, 3 (2003)2416.
[30] F. Jin, F. Sattar, D.Y. Goh, A filter bank-based source extraction algorithm for heart sound removal in respiratory sounds, Comput. Biol. Med. 39 (9) (2009) 768–777.
[31] Z. Wang, J.N. da Cruz, F. Wan, Adaptive Fourier decomposition approach for lung-heart sound separation, in 2015 IEEE International Conference on Computational Intelligence and Virtual Environments for Measurement Systems and Applications (2015)1–5.
[32] L.J. Hadjileontiadis, S.M. Panas, A wavelet-based reduction of heart sound noise from lung sounds, Int. J. Med. Inform. 52 (1) (1998) 183–190.
[33] C. Dimoulas, G. Kalliris, G. Papanikolaou, A. Kalampakas, Novel wavelet domain Wiener filtering de-noising techniques: application to bowel sounds captured by means of abdominal surface vibrations, Biomed. Signal Process. Control 1 (2006) 177–218.
[34] D. Flores-Tapia, Z.M. Moussavi, G. Thomas, Heart sound cancellation based on multiscale products and linear prediction, IEEE Trans. Biomed. Eng. 54 (2) (2007) 234–243.
[35] C. Dimoulas, G. Kalliris, G. Papanikolaou, A. Kalampakas, Long term signal detection, segmentation and summarization using wavelets and fractal dimension: a bioacoustics application in gastrointestinal motility monitoring, Comput. Biol. Med. 37 (2007) 438–462.
[36] C. Dimoulas, G. Papanikolaou, V. Petridis, Pattern classification and audiovisual content management techniques using hybrid expert systems: a video-assisted bioacoustics application in abdominal sounds pattern analysis, Expert Syst. Appl. 38 (2011) 13082–13093.
[37] M.T. Pourazad, Z. Moussavi, G. Thomas, Heart sound cancellation from lung sound recordings using time-frequency filtering, Med. Biol. Eng. Comput. 44 (3) (2006) 216–225.
[38] T. Li, H. Tang, T. Qiu, Y. Park, Heart sound cancellation from lung sound record using cyclostationarity, Med. Eng. Phys. 35 (12) (2013) 1831–1836.
[39] A.A. Sepehri, A. Gharehbaghi, T. Dutoit, A. Kocharian, A. Kiani, A novel method for pediatric heart sound segmentation without using the ECG, Comput. Methods Programs Biomed. 99 (2010) 43–48.
[40] T. Li, H. Tang, T. Qiu, Y. Park, Segmentation of heart sounds based on dynamic clustering, Biomed. Signal Process. Control 7 (2012) 509–516.
[41] Y.L. Tseng, P.Y. Ko, F.S. Jaw, Detection of the third and fourth heart sounds using Hilbert–Huang transform, Biomed. Eng. Online 11 (2012) 1–13.
[42] D. Boutana, B. Barkat, M. Benidir, Segmentation of pathological heart sound signal using empirical mode decomposition, Int. J. Comput. Electr. Eng. 5 (2013) 26–29.
[43] C. Papadaniil, L. Hadjileontiadis, Efficient heart sound segmentation and extraction using ensemble empirical mode decomposition and kurtosis features, IEEE 18 (2014) 1138–1152.
[44] S. Sun, Z. Jiang, H. Wang, Y. Fang, Automatic moment segmentation and peak detection analysis of heart sound pattern via short-time modified Hilbert transform, Comput. Methods Programs Biomed. 114 (2014) 219–230.
[45] A. Mondal, P. Bhattacharya, G. Saha, An automated tool for localization of heart sound components S1, S2, S3 and S4 in pulmonary sounds using Hilbert transform and Heron's formula, Springerplus 2 (1) (2013) 1–14.
[46] N.E. Huang, Z. Shen, S.R. Long, M.C. Wu, H.H. Shih, Q. Zheng, et al., The empirical mode decomposition and Hilbert spectrum for nonlinear and non-stationary time series analysis, Proceedings of Royal Society of London A 454(1998)903–995.
[47] A.O. Andrade, S. Nasuto, P. Kyberd, C.M. Sweeney-Reed, F.R. Van, Kanijn, EMG signal filtering based on empirical mode decomposition, Biomed. Signal Process. Control 1 (1) (2006) 44–55.
[48] L.J. Hadjileontiadis, A novel technique for denoising explosive lung sounds empirical mode decomposition and fractal dimension filter, IEEE 26 (2007) 30–39.
[49] A. Mondal, P.S. Bhattacharya, G. Saha, Reduction of heart sound interference from lung sound signals using empirical mode decomposition technique, J. Med. Eng. Tech. 35 (6–7) (2011) 344–353.
[50] J. Gnitecki, Z. Moussavi, Variance fractal dimension trajectory as a tool for hear sound localization in lung sounds recordings, in Proc. IEEE 25th Annual International Conference of the Engineering in Medicine and Biology Society, 3(2003)2420–2423.
[51] C. Ahlstrom, O. Liljefeldt, P. Hult, P. Ask, Heart sound cancellation from lung sound recordings using recurrence time statistics and nonlinear prediction, IEEE 12 (12) (2005) 812–815.
[52] A. Yadollahi, Z. Moussavi, A robust method for heart sounds localization using lung sounds entropy, IEEE Trans, Biomed. Eng. 53 (3) (2006) 497–502.
[53] F. Jin, F. Sattar, S.G. Razul, D. Goh, Heart sound localization from respiratory sound using a robust wavelet based approach, in Proc. IEEE International Conference on Multimedia and Expo (2008)381–384.

[54] F. Ghaderi, H. Mohseni, S. Sanei, Localizing heart sounds in respiratory signals using singular spectrum analysis, IEEE Trans. Biomed. Eng. 58 (12) (2011) 3360–3367.
[55] R.C. Schlant, R.W. Alexander, Chapter 11, The Heart Arteries and Veins, eighth ed., McGraw Hill Inc., New York, 1998.
[56] P.D. Welch, The use of fast Fourier transform for the estimation of power spectra: a method based on time averaging over short, modified periodograms, IEEE 15 (2) (1967) 70–73.
[57] Y.C. Yeh, W.J. Wang, QRS complexes detection for ECG signal: the difference operation method, Comput. Methods Programs Biomed. 91 (3) (2008) 245–254.
[58] A. Mondal, P.S. Bhattacharya, G. Saha, Detection of lungs status using morphological complexities of respiratory sounds, Sci. World J. 2014 (2014) 1–9.